

Joint Microstrip Selection and Beamforming Design for MmWave Systems with Dynamic Metasurface Antennas

Wei Huang, Haiyang Zhang, Nir Shlezinger, and Yonina C. Eldar

Abstract—Dynamic metasurface antennas (DMAs) provide a new paradigm to realize large-scale antenna arrays for future wireless systems. In this paper, we study the downlink millimeter wave (mmWave) DMA systems with limited number of radio frequency (RF) chains. By using a specific DMA structure, an equivalent mmWave channel model is first explicitly characterized. Based on that, we propose an effective joint microstrip selection and beamforming scheme to accommodate for the limited number of RF chains. A low-complexity digital beamforming solution with channel gain-based microstrip selection is developed, while the analog beamformer is obtained via a coordinate ascent method. The proposed scheme is numerically shown to approach the performance of DMAs without RF chain reduction, verifying the effectiveness of the proposed schemes.

Index terms— Dynamic metasurface antennas, millimeter wave.

I. INTRODUCTION

In order to increase the capacity of wireless communication systems, millimeter wave (mmWave) bands ranging from 30 GHz to 300 GHz, are regarded as a promising candidate. The small wavelength of mmWave signals allows a large number of antenna elements to be packed in a small area, facilitating multiple-input multiple-output (MIMO) processing with very large arrays. However, realizing large antenna arrays for mmWave communication systems in practice can be challenging. A key difficulty stems from the fact that radio frequency (RF) chains in mmWave are costly in terms of hardware implementation, signal processing complexity, and energy consumption. To overcome this issue, various cost-aware hybrid architectures with limited number of RF chains have been proposed [1]–[3]. However, typical hybrid architectures come at the cost of additional analog circuitry, typically comprised of multiple phase shifters, which can lead to relatively high energy consumption [4].

An alternative large-scale MIMO technology utilizes dynamic metasurface antennas (DMAs) [5]. DMAs consist of multiple waveguides (microstrips) and each embedded with many metamaterial antenna elements, which inherently provides analog beamforming capabilities with lower power consumption and cost compared with typical phased array antennas [6]. Moreover, DMAs are typically utilized with sub-wavelength element spacing, allowing to pack a larger number of elements in a given antenna area compared to conventional phased array antennas. This ability has been exploited to improve communication capacity and energy efficiency [7], [8].

Over the last few years, several transmission schemes with DMAs have been studied under various wireless scenarios, such as orthogonal frequency multiplex systems [9], hybrid reconfigurable intelligent surfaces and DMAs network [10], and wireless power transfer [11]. The wireless channels considered in the above works are based on statistical models commonly employed in lower bands, i.e., Rayleigh or Rician distributions. However, for the high-frequency mmWave bandwidth, these models may be not applicable, and one should account for the geometry of the physical channel [12]. In this case,

W. Huang is with the School of Computing Science and Information Engineering, Hefei University of Technology, Hefei, China (e-mail: huangwei@hfut.edu.cn). H. Zhang is with School of Communications and Information Engineering, Nanjing University of Posts and Telecommunications, Nanjing, China (e-mail: 20220142@njupt.edu.cn). N. Shlezinger is with the School of ECE, Ben-Gurion University of the Negev, Beer-Sheva, Israel (e-mail: nirshl@bgu.ac.il). Y. C. Eldar is with the Faculty of Math and CS, Weizmann Institute of Science, Rehovot, Israel (e-mail: yonina.eldar@weizmann.ac.il).

the specific propagation characteristics of DMAs, where signals at different elements propagate differently inside the waveguides [13] is translated into an important consideration for transmission designs in mmWave communication systems. In particular, the equivalent physical channel depends on both the specific DMA structure and mmWave wireless channel model. On the other hand, due to the mmWave channel sparsity, only a small number of beams are needed. Since each beam corresponds to a single RF chain [14], one can use only part of the DMAs microstrips via a switching network, which can further reduce cost and power.

Based on the above observations, in this paper we propose a joint microstrip selection and beamforming design scheme for mmWave signalling with DMAs. We first explicitly characterize the equivalent mmWave physical channel model with a DAM, accounting for the propagation characteristics of mmWave signals and the DAM structure. Based on the obtained equivalent channel model, we then study the hybrid beamforming design problem to maximize the single-noise ratio (SNR), subject to a limit on the number of activated RF chains. The formulated joint microstrip selection and beamforming design problem is non-convex due to both the non-convex l_0 norm constraint and the non-convex Lorentz constraint [15]. To overcome the issue, we develop an iterative algorithm to set the digital beamforming and configure the DMAs weights, alternately. Our optimizer uses a channel-gain based microstrip selection and beamforming, while configuring the DMAs weights via the coordinate ascent method. Simulations result indicate that the proposed scheme could reduce the number of RF chains by 75%, while the spectral efficiency approaches the case without the RF chain constraint.

Notations: In this paper, the upper and lower case bold symbols denote matrices and vectors, respectively. We use $(\cdot)^T$, $(\cdot)^*$, $(\cdot)^H$, $|\cdot|$, and $\|\cdot\|_p$ to denote the transpose, conjugate, Hermitian transpose, absolute value, and p -norm, respectively. $\mathbb{C}^{M \times N}$ is the space of $M \times N$ complex-value matrices, symbol $\angle(\cdot)$ denotes the angle, while \otimes and \odot denote the Kronecker and Hadamard product, respectively.

II. SYSTEM MODEL AND PROBLEM FORMULATION

A. Dynamic Metasurface Antennas

Here, we give a brief review of DMAs. DMAs are metasurface-based antennas comprised of multiple microstrips, which are one-dimensional arrays of metamaterial elements placed on a waveguide cavity [5]. In such architectures, each RF chain is connected with the port located at the edge of the microstrip. Thus, during transmission, the signals in the microstrip propagating from that port undergo a different path for each element, which results in different propagation delay depending on their location. Define α_n as the wavenumber along microstrip n , and $\rho_{n,m}$ denotes the relative location of the m th element of the n th microstrip, which is usually proportional to the distance between the port of microstrip n and the m th element. Thus, element-dependent propagation effect is formulated as

$$f_{n,m} = e^{-\rho_{n,m}(\beta_m + j\alpha_n)}, \forall n, m, \quad (1)$$

where β_m is the waveguide attenuation coefficient of element m .

Each metamaterial elements acts as a resonant circuit whose frequency response for narrowband signaling is approximated as the

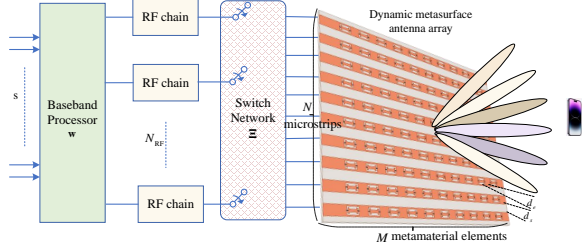


Fig. 1. Downlink MISO system with DMAs.

Lorentzian-constrained phase weights model [13], [16], given by

$$g_{n,m} \in \mathcal{G} \triangleq \left\{ \frac{j + e^{j\phi_{n,m}}}{2} \mid \phi_{n,m} \in [0, 2\pi] \right\}, \forall n, m. \quad (2)$$

Here, $\phi_{n,m}$ denotes the phase shift of the n th element in the m th microstrip. From (1) and (2), we observe that the equivalent DMAs frequency response for each radiating element is a product of the propagation response (1), which is dictated by the placing of the elements, and the tunable Lorentzian phase weight (2).

B. Downlink MmWave Systems with DMAs

We consider a mmWave downlink multiple-input single output (MISO) system as illustrated in Fig. 1. Here, a base station (BS) equipped with a DMA having $U = NM$ radiating metamaterial elements serves a single-antenna user, where N and M denote the number of microstrips and radiating elements in each microstrip, respectively. For cost-effective implementations, the BS is equipped with N_{RF} ($N_{\text{RF}} \leq N$) RF chains, which are connected with the DMA array via a switch network. We adopt the widely utilized geometric block-fading channel model, where the channel from the BS to user, denoted by $\hat{\mathbf{h}} \in \mathbb{C}^{U \times 1}$, is given by

$$\hat{\mathbf{h}} = [\hat{\mathbf{h}}_1^H, \hat{\mathbf{h}}_2^H, \dots, \hat{\mathbf{h}}_n^H \dots, \hat{\mathbf{h}}_N^H]^H = \sum_{l=1}^L \eta_l \mathbf{a}(\theta_l). \quad (3)$$

In (3), $\hat{\mathbf{h}}_n \in \mathbb{C}^{M \times 1}$ denotes the channel from the n th microstrip to user, and L is the number of scatters (paths) from the BS to the user, which is generally much smaller than the number of antennas because of the severe path loss in mmWave band; η_l denotes the complex-value gain of the l th path; $\theta_l \in [0, \pi]$ represents the angle of deviate (AoD) of the l th path between the BS and user; while $\mathbf{a}(\theta_l)$ is the antenna array response vector corresponding to AoD θ_l between BS and user, which is given by

$$\mathbf{a}(\theta_l) = \left[1, \dots, e^{-j \frac{2\pi(M-1)d_e \sin(\theta_l)}{\lambda}} \right]^T \otimes \left[1, \dots, e^{-j \frac{2\pi(N-1)d_s \cos(\theta_l)}{\lambda}} \right]^T \\ = \left[1, \dots, e^{-j \frac{2\pi}{\lambda} \Omega_u(\theta_l)}, \dots, e^{-j \frac{2\pi}{\lambda} \Omega_U(\theta_l)} \right]^T \in \mathbb{C}^U, \quad (4)$$

where λ is the signal wavelength, d_e is the distance between adjacent elements, and d_s denotes the distance between the microstrips. $\Omega_{u=m \cdot N + n}(\theta_l) \triangleq m d_e \sin(\theta_l) + n d_s \cos(\theta_l)$ can be interpreted as the spatial frequency of the u th element corresponding to AoD θ_l .

Since the outgoing signals propagate inside the microstrips before being radiated, the equivalent MISO channel can be represented as

$$\mathbf{h} = [\mathbf{h}_1^H, \dots, \mathbf{h}_N^H]^H = \hat{\mathbf{h}} \odot \mathbf{f} = \left(\sum_{l=1}^L \eta_l \mathbf{a}(\theta_l) \right) \odot \mathbf{f}, \quad (5)$$

with

$$\mathbf{f} = [f_{1,1}, f_{1,2}, \dots, f_{1,M}, \dots, f_{n,m}, \dots, f_{N,M}]^T \in \mathbb{C}^U. \quad (6)$$

The notation $f_{n,m}$ encapsulates the phase due to the distance propagated by the wave from the port of microstrip to the n th element. The vector \mathbf{f} can be interpreted as the array response vector of the

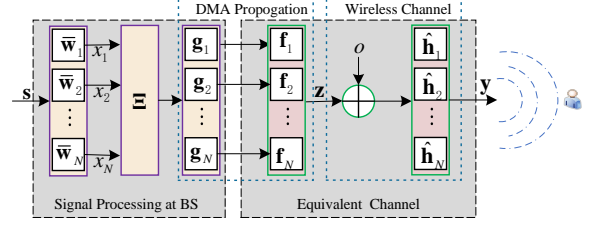


Fig. 2. Illustration of the signal processing procedure.

DMAs. An illustration of the effective channel is depicted in Fig. 2. Differently from conventional phased-array or fully digital architectures, where the propagation characteristic of the wireless channel is not changeable, the outgoing signal undergoes the combined effect of the wireless channel and the microstrips for DMAs, due to the element-dependent propagation inside the microstrip.

For a narrowband mmWave transmitter, the input signal at each microstrip can be expressed as

$$x_n = w_n s, \quad \forall n, \quad (7)$$

where x_n is the input signal for microstrip n , w_n is the corresponding digital beamforming, and s is the information-bearing symbol with normalized power. Then, the baseband signals x_n are fed to the corresponding microstrips via the switch network. Thus, the signal emitting by the m th element in microstrip n is $f_{n,m} z_{n,m}$, where

$$z_{n,m} = g_{n,m} \xi_n x_n = g_{n,m} \xi_n w_n s, \quad (8)$$

where $\xi_n \in \{0, 1\}$ denotes whether the n th microstrip is activated or not. Define the $N \times 1$ vectors $\mathbf{x} = [x_1, \dots, x_N]^H$, $\mathbf{w} = [\xi_1 w_1, \dots, \xi_N w_N]^H$. Then, (8) can be compactly written as

$$\mathbf{z} = \mathbf{G} \mathbf{w} s, \quad (9)$$

where $\mathbf{G} = \text{diag}([\mathbf{g}_1^H, \dots, \mathbf{g}_N^H]) \in \mathbb{C}^{U \times U}$ with $\mathbf{g}_n = [g_{n,1}, \dots, g_{n,M}]^H$ representing the configurable weights of microstrip n . After propagating via the wireless channel, the received signal y is expressed as

$$y = \mathbf{h}^H \mathbf{z} + o = \mathbf{h}^H \mathbf{G} \mathbf{w} s + o, \quad (10)$$

where o is additive white Gaussian noise with variance σ^2 . Then, the achievable rate is given by $\log(1 + \frac{1}{\sigma^2} |\mathbf{h}^H \mathbf{G} \mathbf{w}|^2)$.

C. Problem Formulation

For a mmWave channel with severe path loss, a large-scalar array can be exploited to compensate for the high path loss. Even for a single antenna user, the number of antennas in one microstrip may not be sufficient, that is the fact the emitting energy of back-end antennas will become weaken when the signals are propagating inside the microstrip. It is thus of importance to properly utilize the available RF chains to achieve reliable communications.

Since the number of RF chains at the BS is generally smaller than that of the microstrips in mmWave systems, i.e., $N_{\text{RF}} \leq N$, the RF chains have to selectively connect with some microstrips via the switch network. As such, the number of active microstrips can not exceed N_{RF} . Moreover, as the achievable rate monotonically grows with the SNR, our objective is to maximize the SNR under the RF chains constraint, by joint microstrip selection and beamforming optimization. Therefore, the optimization problem is stated as

$$\max_{\mathbf{w}, \{g_{m,n}\} \in \mathcal{G}} \frac{1}{\sigma^2} |\mathbf{h}^H \mathbf{G} \mathbf{w}|^2 \quad (11a)$$

$$\text{s.t.} \quad \|\mathbf{w}\|_2^2 \leq P \quad (11b)$$

$$\|\mathbf{w}\|_0 \leq N_{\text{RF}}. \quad (11c)$$

Constraint (11c) guarantees that at most N_{RF} microstrips are activated, while (11b) represents the power constraint. Note that problem (11) is non-convex due to the non-convex constraints (11c) and the coupling of optimization variables \mathbf{w} and \mathbf{G} in objective function (11a). Furthermore, different from phased array based hybrid architecture, the analog beamforming of DMAs is subjected to the Lorentz constraint, i.e. $\{g_{n,m}\} \in \mathcal{G}$. To solve the non-convex problem, we develop an iterative algorithm in following section.

III. JOINT MICROSTRIP AND BEAMFORMING DESIGN

In this section, we develop an algorithm to optimize \mathbf{w} and the weights $g_{m,n}$. We adopt an alternating approach, where we maximize the SNR by sequentially fixing one variable and updating the other.

Optimizing \mathbf{w} : For a given \mathbf{G} , the goal is to jointly select the N_{RF} out of N microstrips and design the corresponding beamforming vector associated with the selected microstrips to maximize the SNR. The resultant subproblem is given by

$$\mathcal{P}_1 : \max_{\mathbf{w}} \frac{1}{\sigma^2} |\mathbf{h}^H \mathbf{G} \mathbf{w}|^2 \quad (12a)$$

$$\text{s.t. } \|\mathbf{w}\|_2^2 \leq P \quad (12b)$$

$$\|\mathbf{w}\|_0 \leq N_{\text{RF}}. \quad (12c)$$

Note that in \mathcal{P}_1 , the objective (12a) and power constraint (12b) are convex. The main difficulty lies in the non-convex and non-differentiable cardinality constraint (12c), which restricts the number of the selected microstrips to be no more than N_{RF} . Despite this, \mathcal{P}_1 admits a closed-form solution, as stated in the following:

Proposition 1. Let $\mathcal{I} \triangleq \{i_1, \dots, i_{N_{\text{RF}}}\}$ denote the indices of the N_{RF} largest entries in the set $\{|\mathbf{h}_n^H \mathbf{g}_n|^2\}_{n=1}^N$. Accordingly, define $\bar{\mathbf{h}} \triangleq [\mathbf{h}_{i_1}, \dots, \mathbf{h}_{i_{N_{\text{RF}}}}]$, $\bar{\mathbf{G}} \triangleq \text{diag}([\mathbf{g}_{i_1}^H, \dots, \mathbf{g}_{i_{N_{\text{RF}}}}^H])$, and

$$\bar{\mathbf{w}} = \sqrt{P} \frac{\bar{\mathbf{G}}^H \bar{\mathbf{h}}}{\|\bar{\mathbf{G}}^H \bar{\mathbf{h}}\|}. \quad (13)$$

Then, it holds that \mathcal{P}_1 is solved by setting

$$w_n = \begin{cases} [\bar{\mathbf{w}}]_j & \exists j \in \mathcal{I} \text{ such that } n = i_j \\ 0 & \text{otherwise.} \end{cases} \quad (14)$$

Proof: The proof is given in Appendix A. ■

Optimizing \mathbf{G} : For a given beamforming vector $\bar{\mathbf{w}}$ set via Proposition 1, the resulting SNR is given by

$$\begin{aligned} \text{SNR} &= \frac{1}{\sigma^2} |\bar{\mathbf{h}}^H \bar{\mathbf{G}} \bar{\mathbf{w}}|^2 = \frac{P}{\sigma^2} \|\bar{\mathbf{h}}^H \bar{\mathbf{G}}\|^2 \\ &= \frac{P}{\sigma^2} \sum_{n=1}^{N_{\text{RF}}} \left| \sum_{m=1}^M h_{i_n,m}^* g_{i_n,m} \right|^2, \end{aligned} \quad (15)$$

where $h_{i_n,m}$ denotes the m th element of vector $\mathbf{h}_{i_n,m}$. Then, the configurable weights optimization subproblem is posed as

$$\mathcal{P}_2 : \max_{\{g_{i_n,m}\} \in \mathcal{G}} \frac{P}{\sigma^2} \sum_{n=1}^{N_{\text{RF}}} \left| \sum_{m=1}^M h_{i_n,m}^* g_{i_n,m} \right|^2. \quad (16)$$

Note that in (16), the Lorentzian constraint in \mathcal{P}_2 characterizes the feasible set as a circle on the complex plane $|g - \frac{1}{2} e^{j\frac{\pi}{2}}| = \frac{1}{2}$, with the circle center at $(0, e^{j\frac{\pi}{2}})$ and radius equals to $\frac{1}{2}$. This non-convex constraint makes the subproblem \mathcal{P}_2 difficult to be solved directly. To address the this, we define the variables $b_{n,m}, \forall m, n$, which are related to the DMA weights via the affine mapping

$$b_{n,m} = 2g_{i_n,m} - e^{j\frac{\pi}{2}}, \forall m, n. \quad (17)$$

The variable $b_{n,m}, \forall m, n$ lies on the unit circle of complex plane with the circle center at the origin of coordinates. With (17), the Lorentzian

constraint in \mathcal{P}_2 is converted to the unit-amplitude constraint. Thus, subproblem \mathcal{P}_2 is equivalently transformed into

$$\begin{aligned} \mathcal{P}_{2.1} : \max_{\{b_{n,m}\}} \frac{P}{4\sigma^2} \sum_{n=1}^{N_{\text{RF}}} \left| \sum_{m=1}^M \left(h_{i_n,m}^* b_{i_n,m} + h_{i_n,m}^* e^{j\frac{\pi}{2}} \right) \right|^2 \\ \text{s.t. } |b_{n,m}|^2 = 1, \forall m, n. \end{aligned} \quad (18)$$

While $\mathcal{P}_{2.1}$ is still challenging, it can be tackled via a coordinate ascent-based heuristic algorithm to find a local optimal solution, based on the following proposition.

Proposition 2. Any local optimal phase of (18) satisfies

$$\angle b_{n,m} = -\angle \left(h_{i_n,m}^* \tilde{h}_{n,m} \right) \quad \forall n, m, \quad (19)$$

where $\tilde{h}_{n,m} = \sum_{m' \neq m} h_{i_n,m}^* b_{n,m'} + \sum_{m=1}^M h_{i_n,m}^* e^{j\frac{\pi}{2}}$.

Proof: The proof is given in Appendix B. ■

Using Proposition 2, we can find the local optimal solution of subproblem $\mathcal{P}_{2.1}$ by alternately updating each element $b_{n,m}, n \in \mathcal{I}$, with all other elements fixed. Since the objective function in $\mathcal{P}_{2.1}$ always increases in each iteration, the iteration algorithm can guarantee to converge eventually. Then, based on the affine relationship between $g_{i_n,m}$ and $b_{n,m}$ in (17), we configure the weights of the elements in the active microstrips $\{g_{n,m}\}_{n \in \mathcal{I}}$.

Algorithm Summary: The joint optimization of the DMAs weights along with the microstrip selection and beamforming alternates between the individual settings in Propositions 1-2. In each iteration, we take the solutions $\bar{\mathbf{w}}$ and $\{g_{i_n,m}\}$ into those locations corresponding to the selected microstrips of \mathbf{w} and \mathbf{G} , and set the entries that are non-selected microstrips zeros, respectively. The proposed algorithm to solve problem (11) is summarized as Algorithm 1.

Algorithm 1 Solving problem (11) w.r.t. \mathbf{w} and $\{g_{n,m}\}$

- 1: **Initialize:** set initial \mathbf{G} and threshold $\epsilon > 0$
 - 2: **repeat**
 - 3: Get \mathcal{I} and \mathbf{w} based on \mathbf{G} via Proposition 1;
 - 4: Set $\{g_{n,m}\}_{n \in \mathcal{I}}$ via (19) and (17)
 - 5: **until** SNR increase is smaller than ϵ
 - 6: **Output:** Beampattern \mathbf{w} ; active set \mathcal{I} , and DMA weights $\{g_{n,m}\}$
-

Discussion: The proposed Algorithm 1 jointly designs the digital beamformers, DMA weights, and microstrip selection, via alternating optimization. Each step in Algorithm 1 is based on a simple closed-form computation, and it is particularly designed to be simple to implement such that it can be carried out online. The resulting joint design allows to achieve a rate within a relatively small gap from that of costly fully-digital arrays, as we demonstrate in Section IV.

Our joint design gives rise to multiple potential extensions. The fact that the signal processing capabilities of DMAs can be viewed as a form of hybrid precoding indicates that the proposed Algorithm can be extended to accommodate other forms of hybrid architectures based on, e.g., vector modulators [4] and phase shifter networks [17]. Furthermore, while we focus here on narrowband signalling, for wideband signals, DMAs are known to provide additional degrees of freedom in the form of a flexible frequency selective analog processing [7]. Moreover, when operating in rapidly time-varying channels, one may wish to limit the number of alternating iterations to a small number. In such cases, emerging model-based deep learning techniques [18] can leverage data to facilitate rapid processing, see, e.g., [19]. We leave these extensions for future study.

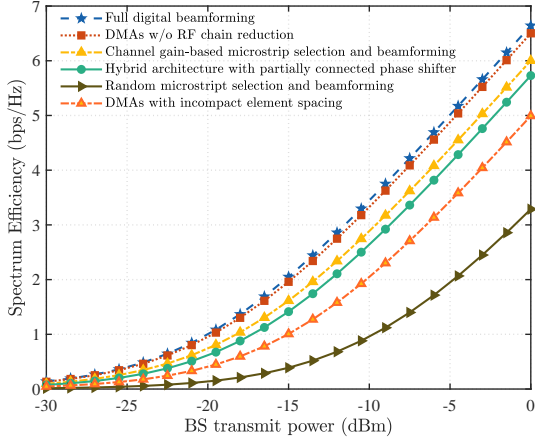


Fig. 3. Spectrum efficiency versus BS transmit power.

IV. NUMERICAL EVALUATIONS

In this section, we numerically evaluate our proposed design. Unless otherwise stated, we consider a planar array located in the xz -plane. All simulated architectures have the same-sized array aperture and the array size is $0.3\text{m} \times 0.3\text{m}$. For DMAs, $\lambda/5$ spacing between the elements inside each microstrip is considered and the separation between microstrips could be still $\lambda/2$. That is, $N = 10$ and $M = 30$. While for the full digital architecture and hybrid architecture with partially connected phase shifter, the element spacing is $\lambda/2$, i.e., $N = M = 10$. The system operates at 28GHz and the mmWave channel has 12 clusters. As in [15], we set $\alpha = 0.6[\text{m}^{-1}]$ and $\beta = 827.67[\text{m}^{-1}]$ to represent the propagation inside the DMA waveguides, representing a microstrip implemented in Duroid 5880.

Our proposed design is compared with the following schemes:

- *Fully digital beamforming*: Each antenna is connected to a dedicated RF chain and the corresponding transmit beamforming uses the maximum ratio transmit (MRT) strategy [20].
- *DMAs architecture without RF chain reduction*: Each microstrip is connected with one RF chain, and the digital and analog beamforming are designed as in [15].
- *DMAs architecture with incompact element spacing*: All elements spacing are set to $\lambda/2$, and the digital and analog beamforming are designed using the approach proposed in Section III.
- *Random microstrip selection and beamforming*: Randomly select the given number of microstrips, and then apply the proposed method in III to design the corresponding digital and analog beamforming.
- *Hybrid architecture with partially connected phase shifter*: The number of connected RF chains is same to the random microstrip selection scheme, and the digital and analog beamforming vectors are derived via the alternate optimization approach proposed in [21].

In Fig. 3, we compare the spectrum efficiency of our proposed Algorithm 1 (channel gain-based microstrip selection and beamforming) with the above-mentioned benchmark schemes. For microstrip reduction schemes, the total number of RF chains is $N_{\text{RF}} = 3$. It is observed that the performance proposed in Algorithm 1 is better than that of the hybrid architecture with partially connected phase shifter. The gain is attributed to the sub-wavelength feature of DMAs, allowing to pack a larger number of elements in a given physical antenna area compared to phased array antennas. However, for DMAs with incompact element space, the performance of hybrid architecture with partially connected phase shifter is better than that of DMAs. Moreover, we can see that the achievable spectrum efficiency of our proposed Algorithm 1 is comparable to that of DMA architecture without RF chain reduction. That is to say, our proposed scheme is

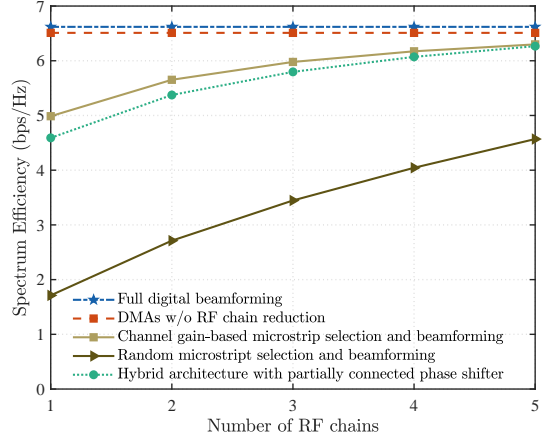


Fig. 4. Spectrum efficiency versus number of RF chains.

capable of reducing the number of RF chains by 75% with negligible performance degradation.

Fig. 4 depicts spectrum efficiency versus the number of RF chains N_{RF} at the BS, where the transmit power is set as 0dBm. It indicates that for all schemes except fully digital and DMA without RF chains reduction, the performance in general improves with more RF chains, but only marginal improvement is observed as N_{RF} exceeds 5. This is expected since performance will be constrained by the number of paths of mmWave channels and size of array aperture. Therefore, by using the proposed joint microstrip selection and beamforming scheme, the DAM can exploit the fewer RF chains to selectively connect to the microstrips so as to attain the performance with the fully RF chains, which can efficiently reduce the cost and power.

V. CONCLUSIONS

In this paper, we studied mmWave MISO communications with DMA and limited number of RF chains. An equivalent mmWave channel model with DMA was characterized. Then, based on this model, a joint optimization problem of DMAs weights, RF chain selection matrix and digital beamforming vector is formulated to maximize the SNR. We proposed an alternating optimization algorithm to solve the non-convex problem. Numerical results show that the proposed scheme can reduce the number of RF chains by 75% and signal processing complexity without compromising on performance.

APPENDIX

A. Proof of Proposition 1:

The SNR expression can be rewritten as

$$|\mathbf{h}^H \mathbf{G} \mathbf{w}|^2 = \sum_{n=1}^N |\mathbf{h}_n^H \mathbf{g}_n w_n|^2 = \sum_{n=1}^N |\mathbf{h}_n^H \mathbf{g}_n|^2 |w_n|^2. \quad (\text{A.1})$$

Thus, to maximize the SNR with the limited number of RF chains ($N = N_{\text{RF}}$), we just need to select N_{RF} largest entries in the set $\{|\mathbf{h}_n^H \mathbf{g}_n|^2\}$ and find the corresponding channels $\bar{\mathbf{h}}$ and DMAs weights $\bar{\mathbf{G}}$. As a result, subproblem \mathcal{P}_1 becomes

$$\mathcal{P}_{1.1}: \max_{\bar{\mathbf{w}}} \frac{1}{\sigma^2} |\bar{\mathbf{h}}^H \bar{\mathbf{G}} \bar{\mathbf{w}}|^2 \quad \text{s.t.} \quad \|\bar{\mathbf{w}}\|_2^2 \leq P, \quad (\text{A.2})$$

where $\bar{\mathbf{w}} \in \mathbb{C}^{N_{\text{RF}} \times 1}$ is the dimension-reduced digital beamforming vector. The optimal solution can be obtained via the MRT, i.e.,

$$\bar{\mathbf{w}}^* = \sqrt{P} \frac{\bar{\mathbf{G}}^H \bar{\mathbf{h}}}{\|\bar{\mathbf{G}}^H \bar{\mathbf{h}}\|}. \quad (\text{A.3})$$

Then, for the selected microstrips, the beamforming coefficients can be extracted from (A.3); otherwise, set it to zero. \square

B. Proof of Proposition 2

Considering the fact that $|b_{n,m}|^2 = 1$ and write it as $e^{j\theta_{n,m}}$, the objective function of (18) can be expanded as

$$\begin{aligned}
 & \sum_{n=1}^{N_{\text{RF}}} \left| \sum_{m=1}^M (h_{i_n,m}^* e^{j\theta_{n,m}} + h_{i_n,m}^* e^{j\frac{\pi}{2}}) \right|^2 = \sum_{n=1}^{N_{\text{RF}}} |h_{i_n,m}^* e^{j\theta_{n,m}} \\
 & + \underbrace{\sum_{m' \neq m} h_{i_n,m}^* e^{j\theta_{n,m'}} + \sum_{m=1}^M h_{i_n,m}^* e^{j\frac{\pi}{2}}}_{\tilde{h}_{n,m}}|^2 \\
 & = \sum_{n=1}^{N_{\text{RF}}} |h_{i_n,m}^* e^{j\theta_{n,m}} + \tilde{h}_{n,m}|^2 = \sum_{n=1}^{N_{\text{RF}}} |h_{i_n,m}^*|^2 + |\tilde{h}_{n,m}|^2 \\
 & + 2\text{Re}\{h_{i_n,m}^* \tilde{h}_{n,m}^* e^{j\theta_{n,m}}\}. \tag{B.1}
 \end{aligned}$$

With all elements of variables $\{b_{n,m}\}$ fixed except $b_{n,m}$, we should maximize $\text{Re}\{h_{i_n,m}^* \tilde{h}_{n,m}^* e^{j\theta_{n,m}}\}$, which is equivalent to minimize the angle between $h_{i_n,m}^* \tilde{h}_{n,m}^*$ and $e^{j\theta_{n,m}}$. Thus, we have

$$\theta_{n,m}^* = -\angle(h_{i_n,m}^* \tilde{h}_{n,m}^*) \quad \forall n, m,$$

which completes the proof. \square

REFERENCES

- [1] R. W. Heath, N. González-Prelcic, S. Rangan, W. Roh, and A. M. Sayeed, "An overview of signal processing techniques for millimeter wave MIMO systems," *IEEE J. Sel. Topics Signal Process.*, vol. 10, no. 3, pp. 436–453, 2016.
- [2] W. Huang, Y. Huang, Y. Zeng, and L. Yang, "Wideband millimeter wave communication with lens antenna array: Joint beamforming and antenna selection with group sparse optimization," *IEEE Trans. Wireless Commun.*, vol. 17, no. 10, pp. 6575–6589, 2018.
- [3] T. Gong, N. Shlezinger, S. S. Ioushua, M. Namer, Z. Yang, and Y. C. Eldar, "RF chain reduction for MIMO systems: A hardware prototype," *IEEE Syst. J.*, vol. 14, no. 4, pp. 5296–5307, 2020.
- [4] T. Zirtoglu, N. Shlezinger, Y. C. Eldar, and R. T. Yazicigil, "Power-efficient hybrid MIMO receiver with task-specific beamforming using low-resolution ADCs," in *IEEE International Conference on Acoustics, Speech and Signal Processing (ICASSP)*, 2022, pp. 5338–5342.
- [5] D. R. Smith, J. B. Pendry, and M. C. Wiltshire, "Metamaterials and negative refractive index," *Science*, vol. 305, no. 5685, pp. 788–792, 2004.
- [6] R. J. Williams, P. Ramírez-Espinosa, J. Yuan, and E. De Carvalho, "Electromagnetic based communication model for dynamic metasurface antennas," *IEEE Trans. Wireless Commun.*, 2022.
- [7] N. Shlezinger, G. C. Alexandropoulos, M. F. Imani, Y. C. Eldar, and D. R. Smith, "Dynamic metasurface antennas for 6G extreme massive MIMO communications," *IEEE Wireless Commun.*, vol. 28, no. 2, pp. 106–113, 2021.
- [8] L. You, J. Xu, G. C. Alexandropoulos, J. Wang, W. Wang, and X. Gao, "Energy efficiency maximization of massive MIMO communications with dynamic metasurface antennas," *IEEE Trans. Wireless Commun.*, 2022.
- [9] H. Wang, N. Shlezinger, Y. C. Eldar, S. Jin, M. F. Imani, I. Yoo, and D. R. Smith, "Dynamic metasurface antennas for MIMO-OFDM receivers with bit-limited adcs," *IEEE Trans. Commun.*, vol. 69, no. 4, pp. 2643–2659, 2021.
- [10] X. Qian, M. Di Renzo, V. Sciancalepore, and X. Costa-Pérez, "Joint optimization of reconfigurable intelligent surfaces and dynamic metasurface antennas for massive MIMO communications," in *IEEE Sensor Array and Multichannel Signal Processing Workshop (SAM)*, 2022, pp. 450–454.
- [11] H. Zhang, N. Shlezinger, F. Guidi, D. Dardari, M. F. Imani, and Y. C. Eldar, "Near-field wireless power transfer with dynamic metasurface antennas," in *IEEE International Workshop on Signal Processing Advances in Wireless Communication (SPAWC)*, 2022.
- [12] O. E. Ayach, S. Rajagopal, S. Abu-Surra, Z. Pi, and R. W. Heath, "Spatially sparse precoding in millimeter wave MIMO systems," *IEEE Trans. Wireless Commun.*, vol. 13, no. 3, pp. 1499–1513, 2014.
- [13] N. Shlezinger, O. Dicker, Y. C. Eldar, I. Yoo, M. F. Imani, and D. R. Smith, "Dynamic metasurface antennas for uplink massive MIMO systems," *IEEE Trans. Commun.*, vol. 67, no. 10, pp. 6829–6843, 2019.
- [14] K. Venugopal, A. Alkhateeb, R. W. Heath, and N. G. Prelcic, "Time-domain channel estimation for wideband millimeter wave systems with hybrid architecture," in *IEEE International Conference on Acoustics, Speech and Signal Processing (ICASSP)*, 2017, pp. 6493–6497.
- [15] H. Zhang, N. Shlezinger, F. Guidi, D. Dardari, M. F. Imani, and Y. C. Eldar, "Beam focusing for near-field multiuser MIMO communications," *IEEE Trans. Wireless Commun.*, vol. 21, no. 9, pp. 7476–7490, 2022.
- [16] D. R. Smith, O. Yurduseven, L. P. Mancera, P. Bowen, and N. B. Kundtz, "Analysis of a waveguide-fed metasurface antenna," *Physical Review Applied*, vol. 8, no. 5, p. 054048, 2017.
- [17] S. S. Ioushua and Y. C. Eldar, "A family of hybrid analog–digital beamforming methods for massive MIMO systems," *IEEE Trans. Signal Process.*, vol. 67, no. 12, pp. 3243–3257, 2019.
- [18] N. Shlezinger, Y. C. Eldar, and S. P. Boyd, "Model-based deep learning: On the intersection of deep learning and optimization," *arXiv preprint arXiv:2205.02640*, 2022.
- [19] O. Agiv and N. Shlezinger, "Learn to rapidly optimize hybrid precoding," in *IEEE International Workshop on Signal Processing Advances in Wireless Communication (SPAWC)*, 2022.
- [20] A. Coskun and C. Candan, "Transmit precoding for flat-fading MIMO multiuser systems with maximum ratio combining receivers," *IEEE Trans. Veh. Tech.*, vol. 60, no. 2, pp. 710–716, 2011.
- [21] J. Zhang, Y. Huang, J. Wang, and L. Yang, "Hybrid precoding for wideband millimeter-wave systems with finite resolution phase shifters," *IEEE Trans. Vehicul. Technology*, vol. 67, no. 11, pp. 11285–11290, 2018.